https://doi.org/10.5194/egusphere-2026-5682
Preprint. Discussion started: 9 November 2026
© Author(s) 2026. CC BY 4.0 License.

BRONet v1.0: A machine learning approach for BrO profile retrieval using a full-physics inverse model

Zhongtao Huang[1], Xin Tian[1,2], Pinhua Xie[2,4,5], Shanshan Wang[3], Yu Huang[1], Zhengde Liu[1], Wenqing Liu[2]

[1]Institutes of Physical Science and Information Technology, Anhui University, Hefei, 230601, China
[2] Anhui Institute of Optics and Fine Mechanics, Hefei Institutes of Physical Science, Chinese Academy of Sciences, Hefei, 230031, China
[3]Shanghai Key Laboratory of Atmospheric Particle Pollution and Prevention (LAP3), Department of Environmental Science and Engineering, Fudan University, Shanghai, 200433, China
[4]Institute of Environment, Hefei Comprehensive National Science Center, Hefei, 230031, China
[5]College of Resources and Environment, University of Chinese Academy of Sciences, Beijing, 101408, China

Correspondence to: Xin Tian (xtian@ahu.edu.cn) and Pinhua Xie (phxie@aiofm.ac.cn)

Abstract. To address the challenge in retrieving tropospheric BrO profiles using the optimal estimation algorithm for Multi-Axis Differential Optical Absorption Spectroscopy (MAX-DOAS)—which relies on a priori profiles—a robust, data-driven retrieval framework, hereafter BRONet v1.0, is developed. First, a comprehensive synthetic dataset comprising 51.5 million samples is generated by coupling physics-based parameterizations of BrO and aerosol profiles with radiative transfer simulations. Second, a hybrid convolutional and long short-term memory neural network (CNN-LSTM) is designed and trained to directly map BrO differential slant column densities (DSCDs) to BrO profiles. This architecture leverages convolutional layers for local feature extraction from multi-angle data and LSTM layers to capture vertical dependencies, enhanced by an attention mechanism for adaptive weighting. The model achieves a coefficient of determination of 0.84 and a root mean square error of 0.36. Finally, the retrieved BrO profiles at Huaniao Island, China, show an average relative deviation of 15.8% compared with those from the optimal estimation algorithm. Notably, the model completes a single profile retrieval in approximately 0.5 s, representing a 240-fold improvement in computational efficiency over the traditional optimal estimation approach, while delivering an enhanced vertical resolution of 191 layers with 10 m resolution below 1 km within the 0-4 km range.

1 Introduction

Tropospheric bromine monoxide (BrO) is recognized as a key atmospheric oxidant, playing a central role in ozone (O3) depletion cycles, the initiation of hydrocarbon oxidation, and the regulation of HOx and NOx cycles (Coburn et al., 2011). Given its high reactivity, the accurate determination of BrO vertical distributions is considered essential for understanding atmospheric oxidation capacity and for identifying critical chemical processes in near-surface ozone pollution (Gliß et al., 2015; Peterson et al., 2015). The inherent challenge in measuring BrO, however, stems from its exceptionally low

https://doi.org/10.5194/egusphere-2026-5682
Preprint. Discussion started: 9 November 2026
© Author(s) 2026. CC BY 4.0 License.

concentrations—typically at parts-per-trillion (ppt) levels, as observed in Antarctic sea ice regions (Wagner et al., 2007), though subject to enhancement during extreme events (Wang et al., 2024a)—coupled with its complex atmospheric interactions.

Multi-Axis Differential Optical Absorption Spectroscopy (MAX-DOAS) has been established as a primary technique for retrieving tropospheric BrO vertical profiles, owing to its operational simplicity and capacity for continuous monitoring (Wagner et al., 2007; Simpson et al., 2017). However, the traditional retrieval framework based on optimal estimation is fundamentally challenged when applied to BrO, due to a compounded dual information bottleneck inherent in the process. The first bottleneck arises during the initial conversion of measured radiance spectra into differential slant column densities (DSCDs), where the extremely weak BrO absorption features are easily obscured by the stronger spectral signatures of absorbers like ozone and nitrogen dioxide. This interference is further compounded by atmospheric scattering effects—including those from aerosols and Rayleigh scattering—as well as additional spectral complexities such as the Ring effect (Simpson et al., 2017; Dubovik et al., 2002), resulting in DSCDs that contain significant and unavoidable uncertainties. The second bottleneck occurs in the subsequent retrieval step, where the vertical concentration profile is estimated from these noisy DSCDs. This constitutes a severely ill-posed problem, typically solved by coupling a physical forward model (e.g., the radiative transfer model SCIATRAN) with an optimal estimation algorithm. The solution is highly sensitive to a priori constraints and regularization choices; under the low signal-to-noise conditions characteristic of BrO, this sensitivity can introduce substantial biases and lead to significant retrieval uncertainties, particularly in the critical near-surface region where BrO chemistry is most active and light paths are most complex (Dubovik et al., 2002; Hönninger et al., 2003).

Machine learning has emerged as a promising alternative paradigm, capable of directly learning complex nonlinear relationships between observations and atmospheric states from data (Sellitto et al., 2011; Zhang et al., 2024). Its application extends beyond trace gas retrieval, having been successfully adopted across various remote sensing domains where it demonstrates substantial advantages in handling high-dimensional data and intricate physical processes (Frieß et al., 2019; Hedelt et al., 2019; Schilling et al., 2018; Efremenko et al., 2017). Recent studies have validated the potential of deep learning for atmospheric profile retrieval: for aerosol profiles (Dong et al., 2020), for tropospheric NO2 profiles from MAX-DOAS spectra using a hybrid CNN-SVR model (Pan et al., 2022), and for high-resolution ozone profiles using ensemble methods and convolutional neural networks (CNNs) (Wang et al., 2024b). These advances underscore the potential of data-driven approaches to capture the nuances of radiative transfer.

Nevertheless, the performance of machine learning models is critically dependent on access to large-scale, high-quality training datasets with precise input–output pairs (Dong et al., 2020). For BrO retrieval, this requirement presents a fundamental obstacle due to the scarcity of comprehensive, co-located vertical profile measurements. Existing observational datasets capture only a limited subset of possible atmospheric states, which severely constrains the generalization capability of models trained on them. To overcome the critical limitation of data scarcity and to directly address the second bottleneck—the ill-posed retrieval step—this study develops a novel approach centered on the generation of a comprehensive synthetic dataset via physics-based radiative transfer modeling. Based on this comprehensively sampled

https://doi.org/10.5194/egusphere-2026-5682
Preprint. Discussion started: 9 November 2026
© Author(s) 2026. CC BY 4.0 License.

synthetic dataset, a hybrid neural network architecture is designed. This integrated design is tailored to address the dual challenges of performing robust feature extraction from potentially noisy input DSCDs and of modeling the contextual continuity inherent in vertical profile structures (Bartlett and Baxter, 2002; Gers et al., 2000).

This paper is structured as follows. Section 2 presents the methodology, including the overall framework, synthetic dataset construction, and the rationale for the machine-learning approach and data preprocessing. Section 3 details the hybrid CNN-LSTM model architecture, training configuration, and implementation. Section 4 evaluates the model performance on synthetic data, its generalization to unseen scenarios, and its validation using real MAX-DOAS observations. Section 5 discusses the key findings, advantages over traditional retrieval methods, and limitations, while Section 6 provides concluding remarks.

2 Methodology

2.1 Overall Research Framework

The comprehensive framework of this study comprises three interconnected and sequentially dependent components (Fig. 1). Firstly, a comprehensive training dataset is generated through a physics-based parameterization of atmospheric states, coupled with rigorous radiative transfer simulations performed using the SCIATRAN model (Rozanov et al., 2005). This process systematically generates diverse BrO vertical profiles and their corresponding MAX-DOAS observational data, which include the DSCD sequences, solar geometry, and aerosol extinction profiles, thereby establishing precise physical mappings between atmospheric states and observational signals. Secondly, a specialized hybrid CNN-LSTM architecture (BRONet v1.0), engineered for the MAX-DOAS BrO retrieval problem, is designed and trained. This model directly learns the inverse mapping from multi-angle DSCDs and auxiliary parameters to BrO vertical concentration profiles. Lastly, a multi-faceted validation approach is implemented. This encompasses internal validation performed on synthetic data, generalization testing conducted with unseen parameter combinations, and external validation carried out using real MAX-DOAS observations, ensuring the reliability and practical utility of the proposed machine learning approach.

https://doi.org/10.5194/egusphere-2026-5682
Preprint. Discussion started: 9 November 2026
© Author(s) 2026. CC BY 4.0 License.

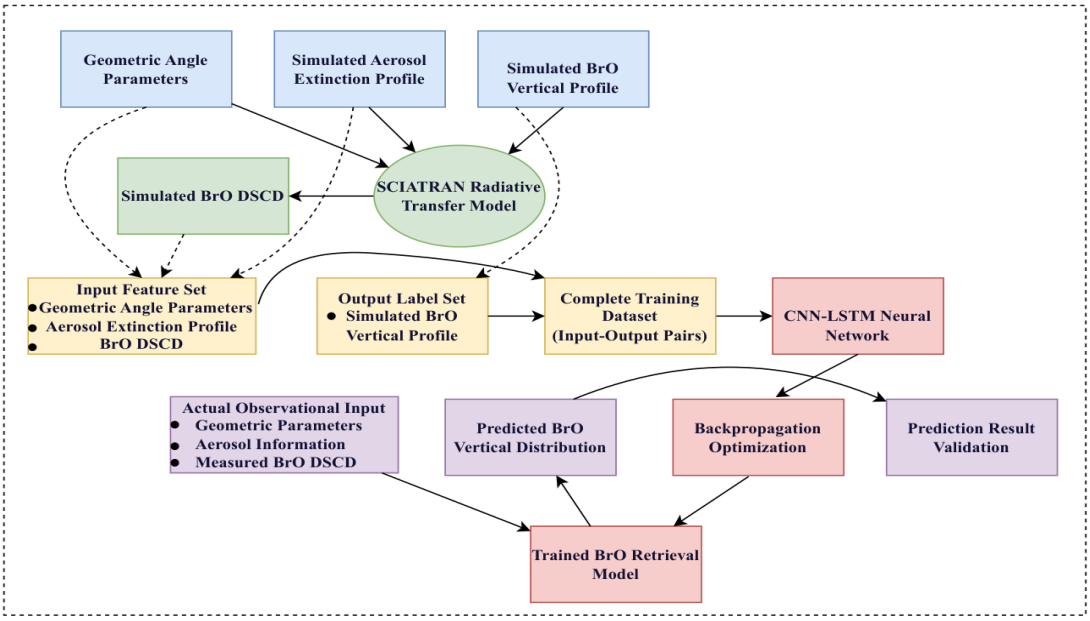


Figure 1. Overall research framework of this study, comprising three core components: (1) physics-based parameterization of BrO and aerosol vertical profiles, coupled with SCIATRAN radiative transfer simulations to generate a comprehensive synthetic dataset; (2) design and training of a neural network to learn the inverse mapping from BrO differential slant column densities (DSCDs) to BrO vertical profiles; and (3) a multi-faceted validation strategy.

2.2 Construction of synthetic datasets

2.2.1 MAX-DOAS Measurement Principles and Retrieval Physics

The MAX-DOAS technique retrieves vertical profiles of atmospheric trace gases by analyzing scattered sunlight received from multiple viewing directions. Its fundamental principle relies on the differential absorption characteristics of the target gas at specific wavelengths, and the peak absorption wavelength of BrO is 350 nm.

Traditional MAX-DOAS trace gas profile retrieval typically involves a two-step process: first, obtaining the differential slant column densities (DSCDs) of the target gas through spectral fitting; second, inputting these gas DSCDs along with atmospheric state parameters into a profile retrieval algorithm built upon an atmospheric radiative transfer model to retrieve the trace gas vertical profile and vertical column density (Hönninger et al., 2003). Within this framework, the DSCD sequence at multiple elevation angles provides the most direct differential absorption information; the solar geometry, comprising the solar zenith angle (SZA) and relative azimuth angle (RAA), where the SZA controls the incident solar radiation path length and atmospheric penetration depth, and the RAA influences the spatial relationship between the light path and gas distribution under horizontal inhomogeneity; and the aerosol optical properties, including the aerosol extinction profile, the single scattering albedo (SSA), and the asymmetry factor, which collectively modulate the light path

https://doi.org/10.5194/egusphere-2026-5682
Preprint. Discussion started: 9 November 2026
© Author(s) 2026. CC BY 4.0 License.

enhancement factor through scattering and absorption processes, particularly critical for low-elevation observations. Therefore, the sensitivity of DSCDs to trace gas vertical distributions depends not only on the gas concentration itself but also on the observation geometry and the aerosol loading and microphysical properties, which together determine the light path and radiative transfer effects (Dong et al., 2020; Dubovik et al., 2002).

2.2.2 Radiative Transfer Modeling with SCIATRAN

To generate comprehensive training data that spans the wide range of possible atmospheric conditions, we parameterized BrO vertical profiles using three physically meaningful mathematical distributions (exponential, Gaussian, and Boltzmann), each representing distinct atmospheric scenarios commonly observed in the troposphere (Tian et al., 2021). The gas profile state parameters are shown in Table 1 and Table 2 (Wagner et al., 2007; Wang et al., 2024a).

Table 1. BrO prior state parameter settings.

Parameter	Values
Target gas	BrO
Vertical grid	10 m vertical resolution at altitudes below 1.0 km, 20 m vertical resolution at altitudes from 1.0 to 2.0 km, and 50 m vertical resolution at altitudes from 2.0 to 4.0 km
Vertical column density (10^{14} molec. cm^{-2})	0.05, 0.1, 0.15, 0.2, 0.3, 0.4, 0.5, 0.7, 0.9, 1.5, 3.0, 5.0
Profile type and parameters	Exponential: scale heights 0.2, 0.5, 1.0 km; Boltzmann: heights 1.0, 1.5, 2.0 km; Gaussian: peak heights 0.5, 1.0 km, peak widths 0.2, 0.5, 1.0, 1.5 km

Table 2. Aerosol prior state parameter settings.

Parameter	Values
Target gas	Aerosol
Vertical grid	200 m resolution at an altitude range below 4.0 km
Aerosol optical depth	0.15, 0.3, 0.45, 0.6, 0.75, 0.9, 1.0, 1.5, 2.0, 2.5, 3.0, 4.0, 5.0
Single scattering albedo (SSA)	0.7, 0.75, 0.8, 0.85, 0.9, 0.95, 1.0
Asymmetry parameter (AP)	0.68, 0.72, 0.78, 0.82
Profile type and parameters	Exponential: scale heights 0.2, 0.5, 0.8, 1.0 km; Boltzmann: heights 0.5, 1.0, 1.5, 2.0 km; Gaussian: peak heights 0.5, 1.0 km, peak widths 0.2, 0.5, 1.0, 1.5 km

The atmospheric states generated through the parameterization process described above were used as inputs to the SCIATRAN radiative transfer model (version 2.2) to simulate realistic MAX-DOAS observations (Rozanov et al., 2005).

https://doi.org/10.5194/egusphere-2026-5682
Preprint. Discussion started: 9 November 2026
© Author(s) 2026. CC BY 4.0 License.

SCIATRAN is a comprehensive radiative transfer code that numerically solves the radiative transfer equation for a plane-parallel atmosphere, accounting for multiple scattering, absorption, and polarization effects. In the radiative transfer simulations, we used the Standard Atmosphere for temperature, pressure, and ozone profiles, consistent with the approach in the original MAX-DOAS studies (Tian et al., 2021). The incident solar spectrum at the top of the atmosphere was specified using a standard solar spectrum (ATLAS). The surface albedo was set to 0.06, representing typical land/vegetation conditions. A comprehensive set of viewing geometries was simulated to cover the full range of possible observational conditions. The key parameters used in the radiative transfer simulations are summarized in Table 3. These parameter ranges were selected to cover the full scope of possible observational conditions, from near-zenith sun positions to large solar zenith angles characteristic of high-latitude measurements, and from small relative azimuth angles (near the principal plane) to large angles (near the perpendicular plane). The radiative transfer simulations produced a dataset of over 51.5 million independent samples, with each sample forming a complete input–output pair for supervised learning.

Table 3. Key parameter settings for the SCIATRAN radiative transfer simulations.

Parameter category	Values / specification
Central wavelength (nm)	350 (focused on BrO absorption features)
Solar zenith angle (SZA; °)	10, 20, 30, 40, 50, 60, 70, 80, 85, 89
Relative azimuth angle (RAA; °)	10, 20, 40, 60, 80, 100, 120, 140, 160, 180
Elevation angles (EA; °)	1, 2, 3, 4, 5, 6, 8, 15, 30, 90
Surface albedo	0.06 (typical for land/vegetation)
Standard atmospheric profiles	Standard Atmosphere (for temperature, pressure, and humidity) (Rozanov et al., 2005)
Incident solar spectrum	Standard solar spectrum (ATLAS) used as top-of-atmosphere source

The generated input–output pairs were subsequently used for supervised machine learning, where the input is defined as follows. The input is a 32-dimensional vector consisting of the following components: the solar zenith angle (SZA) and the relative azimuth angle (RAA), which define the solar geometry; a sequence of nine BrO differential slant column densities (DSCDs) corresponding to the elevation angles 1, 2, 3, 4, 5, 6, 8, 15, and 30°; and a 21-value aerosol extinction coefficient profile defined on a regular vertical grid from the surface to 4.0 km altitude with a constant 200 m resolution. The output target is the BrO number density vertical profile, represented as a 191-dimensional vector. The profile is defined on a variable-resolution vertical grid with a spacing of 50 m from 4.0 km down to 2.0 km, 20 m from 2.0 km down to 1.0 km, and 10 m below 1.0 km. It covers altitudes from the surface up to 4.0 km, with the first vector element corresponding to the topmost layer at 4.0 km.

https://doi.org/10.5194/egusphere-2026-5682
Preprint. Discussion started: 9 November 2026
© Author(s) 2026. CC BY 4.0 License.

2.3 Machine Learning Models and Data Preprocessing

2.3.1 Rationale for Machine Learning Approach Selection

Machine learning provides an alternative paradigm by directly learning the inverse mapping from observations to atmospheric states. Our approach integrates three complementary deep learning architectures, each selected to address specific aspects of the MAX-DOAS BrO retrieval problem.

CNNs excel at extracting localized patterns through hierarchical filter-based processing. In this application, 1D convolutional layers effectively identify subtle BrO absorption signatures within multi-angle DSCD sequences. The filters learn characteristic patterns correlated with different vertical distribution features, which is crucial for distinguishing weak BrO signals from measurement noise and atmospheric interference (Dong et al., 2020; Bartlett and Baxter, 2002). Long short-term memory networks (LSTMs) specialize in modeling sequential dependencies through gated memory mechanisms, making them ideal for representing the continuous vertical variation of BrO concentrations. The bidirectional LSTM (Bi-LSTM) used here processes sequences in both forward and backward directions, capturing contextual dependencies across altitudes while mitigating the vanishing gradient problem (Gers et al., 2000; Tian et al., 2022). Attention mechanisms enable dynamic weighting of input features, allowing the model to focus adaptively on the most informative observational angles and auxiliary parameters for each altitude level. This is particularly valuable given the nonlinear relationship between DSCDs and vertical profiles and the varying sensitivity of different elevation angles.

The integration of CNN, LSTM, and attention mechanisms provides a comprehensive solution, simultaneously addressing feature extraction from noisy observations, sequence modeling of vertical dependencies, and adaptive information weighting. This hybrid design leverages the complementary strengths of each component to achieve robust and accurate profile retrievals.

2.3.2 Data Preprocessing

To ensure data quality and compatibility with machine learning algorithms, the raw simulated data underwent rigorous preprocessing, encompassing quality control, standardization, and dataset partitioning.

First, a quality control step was applied to remove physically unrealistic samples. This involved filtering out instances with negative BrO number densities or aerosol extinction coefficients, values which may arise from numerical instabilities in the radiative transfer simulations or extreme parameter combinations.

Subsequently, Z-score standardization was independently applied to each input feature and output target to normalize the data to a mean of zero and a standard deviation of one (Wang et al., 2024b). The transformation is defined as:

$$x_{norm} = (x - \mu)/\sigma \quad (1)$$

https://doi.org/10.5194/egusphere-2026-5682
Preprint. Discussion started: 9 November 2026
© Author(s) 2026. CC BY 4.0 License.

where μ and σ represent the arithmetic mean and standard deviation of each feature computed across the entire dataset. This step is crucial as it ensures all features contribute equally to the model's learning process and promotes faster training convergence.

Finally, the processed dataset was randomly partitioned into a training set (85%, approximately 43.8 million samples) and a validation set (15%, approximately 7.7 million samples). Stratified sampling was employed to maintain consistent distributions of BrO profile shapes, aerosol loadings, and observation geometries across both sets, thereby preventing bias in the subsequent model evaluation.

This comprehensive and preprocessed dataset reliably establishes the physical mapping from multi-angle DSCD observation vectors and auxiliary parameters to BrO vertical distributions. It provides an essential foundation for training the machine learning models described in the following section, ensuring the approach is grounded in physically consistent simulation data spanning a wide range of atmospheric conditions.

3 Machine Learning Model Development

3.1 Model Architecture Design

Based on the theoretical considerations outlined in Sect. 2, we designed BRONet v1.0, a hybrid neural network architecture that integrates 1D CNNs, bidirectional long short-term memory (Bi-LSTM) networks, and attention mechanisms. The complete architecture, illustrated in Fig. 2, employs an encoder–decoder framework specifically engineered to address the dual challenges of feature extraction from multi-angle observations and contextual understanding of vertical profile structures.

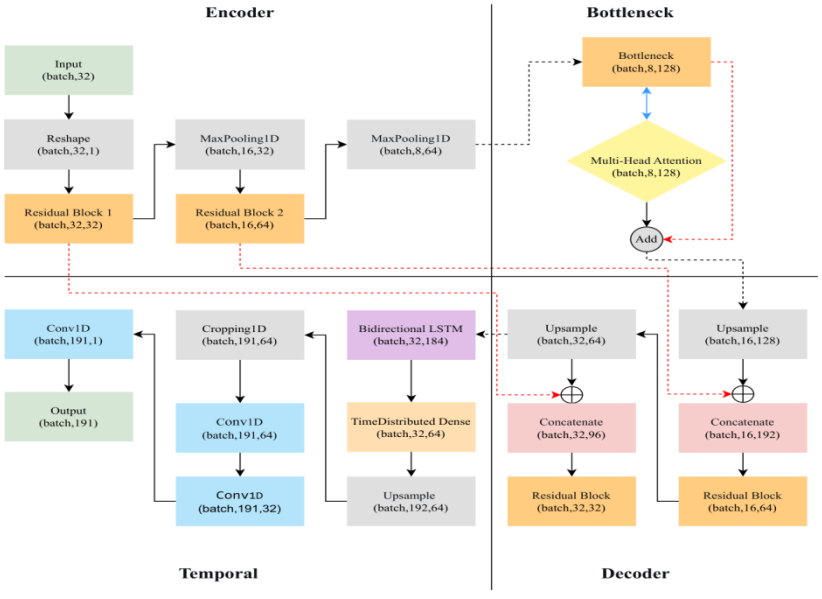


Figure 2. Hybrid CNN-LSTM architecture with attention mechanism.

https://doi.org/10.5194/egusphere-2026-5682
Preprint. Discussion started: 9 November 2026
© Author(s) 2026. CC BY 4.0 License.

The model first processes the 32-dimensional input feature vector through an encoder module based on convolutional operations for hierarchical feature extraction. The encoder comprises two cascaded residual convolutional blocks, each followed by max-pooling to reduce spatial dimensionality. Each residual block contains a 1D convolutional layer (using 32 and 64 filters with a kernel size of 3 in the first and second block, respectively), batch normalization to stabilize training, a ReLU activation function to introduce nonlinearity, and dropout regularization with a rate of 0.3 to prevent overfitting. Skip connections within these blocks mitigate the vanishing gradient problem by allowing gradients to flow directly through the network. Following this, a third residual convolutional block with 128 filters forms a bottleneck stage, creating a compressed representation that captures the essential patterns from the multi-angle DSCDs and aerosol profiles relevant for BrO retrieval. Subsequently, the bottleneck features pass through a lightweight multi-head self-attention layer with 4 attention heads and a key dimension $d_k = 32$. This mechanism enhances the model's ability to adaptively weight the importance of different input features. It computes a weighted sum where the weights are determined by the compatibility between different parts of the input sequence, as defined by:

$$\begin{aligned} \mathrm{MultiHead}(Q, K, V) &= \mathrm{Concat}(\mathrm{head}_1, \ldots, \mathrm{head}_h)\, W^O \\ \text{where } \mathrm{head}_i &= \mathrm{Attention}(Q\, W_i^Q, K\, W_i^K, V\, W_i^V) \\ \mathrm{Attention}(Q, K, V) &= \mathrm{softmax}(Q\, K^T / \sqrt{d_k})\, V \end{aligned} \tag{2}$$

Here, Q, K, and V represent the queries, keys, and values matrices derived from the input features; W_i^Q, W_i^K, and W_i^V are the learned projection matrices for head i; and W^O is the output projection matrix.

The attended features are then processed by a decoder that reconstructs the spatial resolution through upsampling. The decoder consists of two stages, each combining upsampled features with skip connections from corresponding encoder layers via concatenation. Each stage employs a residual convolutional block (with 64 and 32 filters, respectively) to refine the feature representations.

The decoded features are then fed into a bidirectional long short-term memory (Bi-LSTM) network with 92 units in each direction to capture the contextual dependencies inherent in the vertical dimension. The LSTM unit implements gating mechanisms at each time step t, governed by the following equations:

$$\begin{aligned} f_t &= \sigma(W_f \cdot [h_{t-1}, x_t] + b_f) \quad \text{(Forget gate)} \\ i_t &= \sigma(W_i \cdot [h_{t-1}, x_t] + b_i) \quad \text{(Input gate)} \\ \tilde{C}_t &= \tanh(W_C \cdot [h_{t-1}, x_t] + b_C) \quad \text{(Candidate cell state)} \\ C_t &= f_t \odot C_{t-1} + i_t \odot \tilde{C}_t \quad \text{(Cell state update)} \\ o_t &= \sigma(W_o \cdot [h_{t-1}, x_t] + b_o) \quad \text{(Output gate)} \\ h_t &= o_t \odot \tanh(C_t) \quad \text{(Hidden state)} \end{aligned} \tag{3}$$

https://doi.org/10.5194/egusphere-2026-5682
Preprint. Discussion started: 9 November 2026
© Author(s) 2026. CC BY 4.0 License.

where x_t is the input, h_{t-1} is the previous hidden state, C_{t-1} is the previous cell state, W and b are learned weights and biases, σ is the sigmoid function, tanh is the hyperbolic tangent, and ⊙ denotes element-wise multiplication. The bidirectional architecture processes the sequence in both forward and backward directions, providing comprehensive contextual information.

Finally, the features from the Bi-LSTM network undergo a final upsampling via linear interpolation (with a factor of 6) to match the target output dimension of 191, followed by cropping to the exact length. The upsampled features are then processed through three consecutive 1D convolutional layers (with 64, 32, and 1 filter, respectively). The first two layers use ReLU activation, while the final layer uses a linear activation function. The output is flattened to produce the final 191-dimensional prediction of the BrO concentration profile.

The complete model architecture contains approximately 375,000 trainable parameters, achieving an efficient balance between representational capacity and computational cost.

3.2 Training Configuration and Optimization

The model was implemented in TensorFlow 2.15 with mixed-precision training enabled to accelerate computation. We employed the Adam optimizer with an initial learning rate of 1×10^{-6}, gradient clipping (global norm 1.0), and a learning-rate schedule that combined warm-up and cosine decay. Training used a batch size of 512 and was run for up to 100 epochs; early stopping (patience 15 epochs) was applied based on the validation loss. The model was trained to minimize the mean squared error (MSE) loss,

$$L_{MSE} = (1/N) \Sigma_{i=1}^{N} (y_i - \hat{y}_i)^2 \quad (4)$$

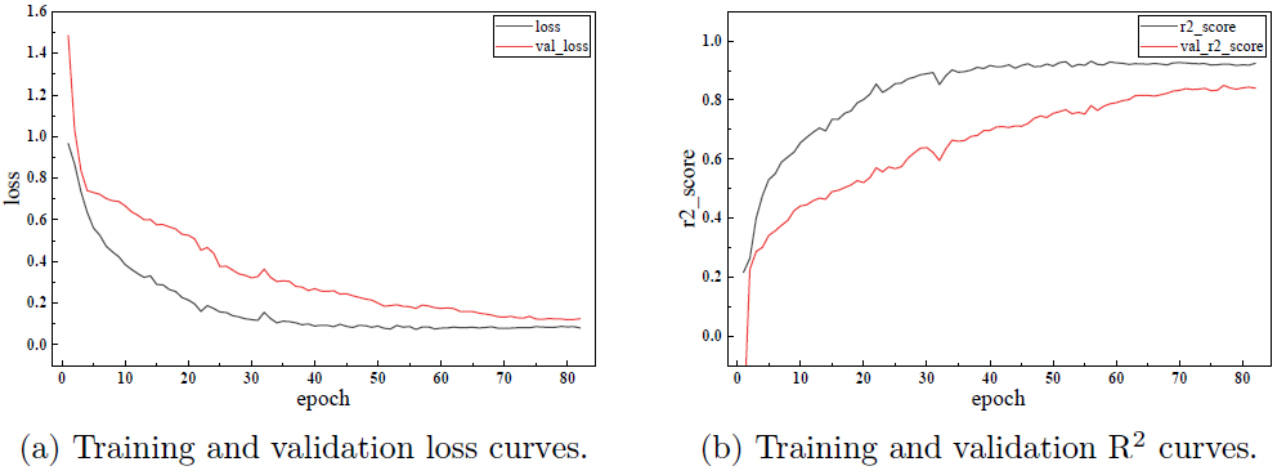
where y_i denotes the true BrO profile, $\hat{y}_i$ the predicted profile, and N the batch size. Regularization included L2 weight decay ($\lambda = 0.001$), dropout (rate 0.3), and batch normalization.

The synthetic dataset of 51.5 million samples was split into training (85%) and validation (15%) sets, ensuring similar distributions of BrO profiles, aerosol loadings, and observation geometries. A custom data-loading pipeline with buffering and on-demand reading from Apache Parquet files was used to handle the large-scale data efficiently. Model checkpoints were saved every epoch, and the checkpoint with the lowest validation loss was selected for final evaluation.

Performance was evaluated primarily by the coefficient of determination (R^2), supplemented by the root mean square error (RMSE).

$$R^2 = 1 - \Sigma_{i=1}^{n} (y_i - \hat{y}_i)^2 / \Sigma_{i=1}^{n} (y_i - \bar{y})^2 \quad (5)$$

https://doi.org/10.5194/egusphere-2026-5682
Preprint. Discussion started: 9 November 2026
© Author(s) 2026. CC BY 4.0 License.



(a) Training and validation loss curves. (b) Training and validation R^2 curves.

Figure 3. Model training performance metrics. (a) Mean squared error loss as a function of training epochs for both training and validation sets. (b) Coefficient of determination (R^2) as a function of training epochs for both sets.

4 Comparison and Validation

4.1 Machine Learning Model Performance on Synthetic Data

The hybrid CNN-LSTM model effectively learned the mapping from multi-angle DSCDs and auxiliary parameters to BrO vertical profiles. On the training set (43.8 million samples), the model achieved an R^2 of 0.92 and an RMSE of 0.28 (the square root of MSE). Its performance on the independent validation set (7.7 million samples) remained strong, with an R^2 of 0.84 and an RMSE of 0.36, explaining 84% of the variance in unseen data (Fig. 3). The gap between training and validation metrics indicates mild overfitting—consistent with the model's complexity—while confirming its substantial generalization capability. Figure 3 illustrates the convergence of the training and validation loss (MSE), alongside the corresponding R^2 trends, demonstrating stable learning and effective optimization.

4.2 Generalization to Unseen Atmospheric Scenarios

To evaluate the model's generalization ability beyond the training distribution, we tested it on nine scenarios with parameter combinations explicitly excluded during training. All scenarios shared identical aerosol properties and observation geometry, varying only in BrO profile morphology and vertical column density (VCD), as detailed in Table 4. Across all tests, the model achieved excellent performance, with the coefficient of determination (R^2) consistently above 0.96, indicating it learned the underlying mapping rather than memorizing the training set.

Table 4. Configuration and performance metrics of new simulation test scenarios.

Scenario	Profile type	Key parameter settings	R^2

https://doi.org/10.5194/egusphere-2026-5682
Preprint. Discussion started: 9 November 2026
© Author(s) 2026. CC BY 4.0 License.

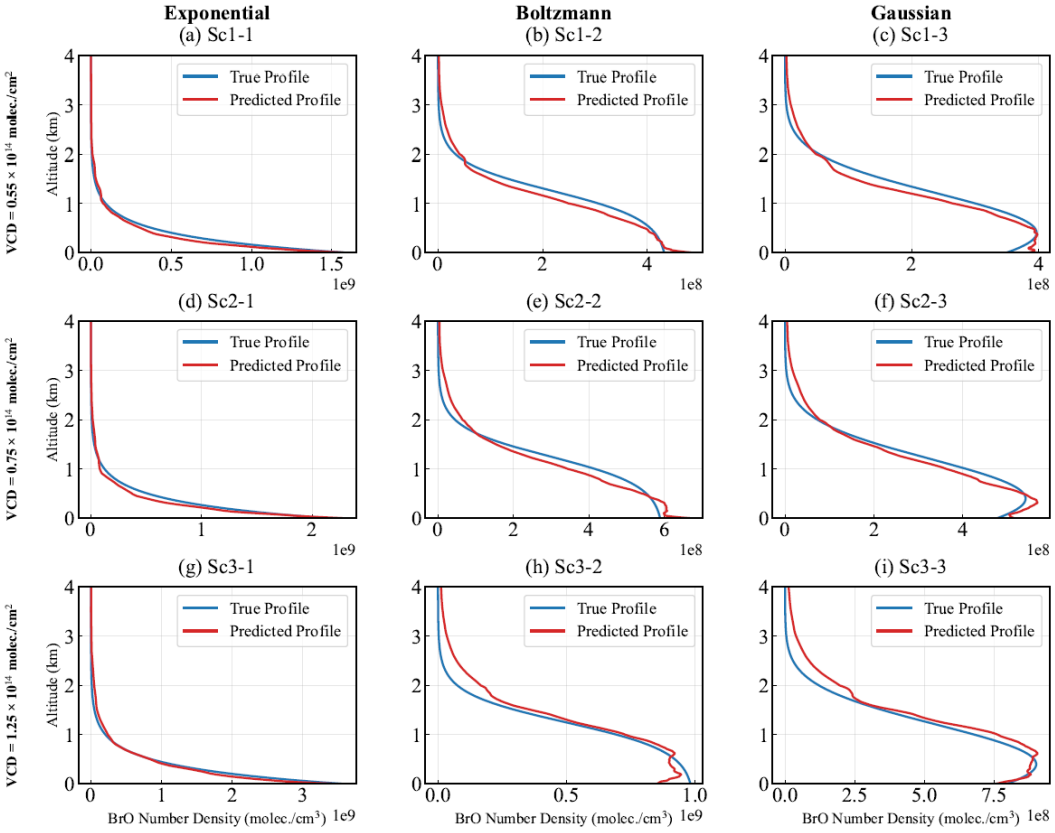
Sc1-1	Exponential	Scale height = 0.35 km, VCD = 0.55 × 10^{14} molec. cm^{-2}	0.96
Sc2-1	Exponential	Scale height = 0.35 km, VCD = 0.75 × 10^{14} molec. cm^{-2}	0.97
Sc3-1	Exponential	Scale height = 0.35 km, VCD = 1.25 × 10^{14} molec. cm^{-2}	0.97
Sc1-2	Boltzmann	BL height = 1.25 km, VCD = 0.55 × 10^{14} molec. cm^{-2}	0.97
Sc2-2	Boltzmann	BL height = 1.25 km, VCD = 0.75 × 10^{14} molec. cm^{-2}	0.97
Sc3-2	Boltzmann	BL height = 1.25 km, VCD = 1.25 × 10^{14} molec. cm^{-2}	0.98
Sc1-3	Gaussian	Peak height = 0.4 km, peak width = 0.8 km, VCD = 0.55 × 10^{14} molec. cm^{-2}	0.98
Sc2-3	Gaussian	Peak height = 0.4 km, peak width = 0.8 km, VCD = 0.75 × 10^{14} molec. cm^{-2}	0.98
Sc3-3	Gaussian	Peak height = 0.4 km, peak width = 0.8 km, VCD = 1.25 × 10^{14} molec. cm^{-2}	0.98

A quantitative analysis combining profile comparisons (Fig. 4) and percentage deviation distributions (Fig. 5) reveals key performance patterns. Inversion accuracy depends on profile morphology: Gaussian profiles were retrieved most accurately (mean NRMSE 9.2%), followed by Boltzmann (mean NRMSE 10.8%) and exponential profiles (mean NRMSE 11.2%). Exponential profiles with low VCD posed the greatest challenge (NRMSE 12.3% in Scenario 1-1).

Model performance improved systematically with increasing VCD. As VCD rose from 0.55 to 1.25 × 10^{14} molec. cm^{-2}, the average NRMSE decreased from 11.3% to 9.1%, likely because higher column densities produce stronger differential absorption signals with better signal-to-noise ratios for the model to exploit.

Vertical error distributions show systematic patterns. For exponential profiles, negative deviations (underestimation) dominate near the surface (average Signed MNAE 5.6%). For Boltzmann and Gaussian profiles, slight positive deviations (overestimation) often occur near the boundary layer top (≈1.5–2.0 km). This smoothing tendency is characteristic of data-driven models fitting complex nonlinear functions and may reflect interpolation for boundary layer heights (e.g., 1.25 km) not seen during training. Maximum absolute deviations typically occur at altitude layers with the sharpest concentration gradients, yet most deviations remain within 20%, demonstrating the model's robustness in reconstructing vertical structures.

https://doi.org/10.5194/egusphere-2026-5682
Preprint. Discussion started: 9 November 2026
© Author(s) 2026. CC BY 4.0 License.



290 **Figure 4.** Comparison of retrieved and true BrO vertical profiles for nine unseen test scenarios arranged in a 3 × 3 layout. Columns correspond to different BrO profile types: (a, d, g) exponential, (b, e, h) Boltzmann, and (c, f, i) Gaussian. Rows correspond to different vertical column densities (VCDs): (a, b, c) 0.55, (d, e, f) 0.75, and (g, h, i) 1.25 × 10^{14} molec. cm^{-2}. Solid blue lines represent the simulated true profiles; red lines represent the predictions from the deep learning model.

https://doi.org/10.5194/egusphere-2026-5682
Preprint. Discussion started: 9 November 2026
© Author(s) 2026. CC BY 4.0 License.

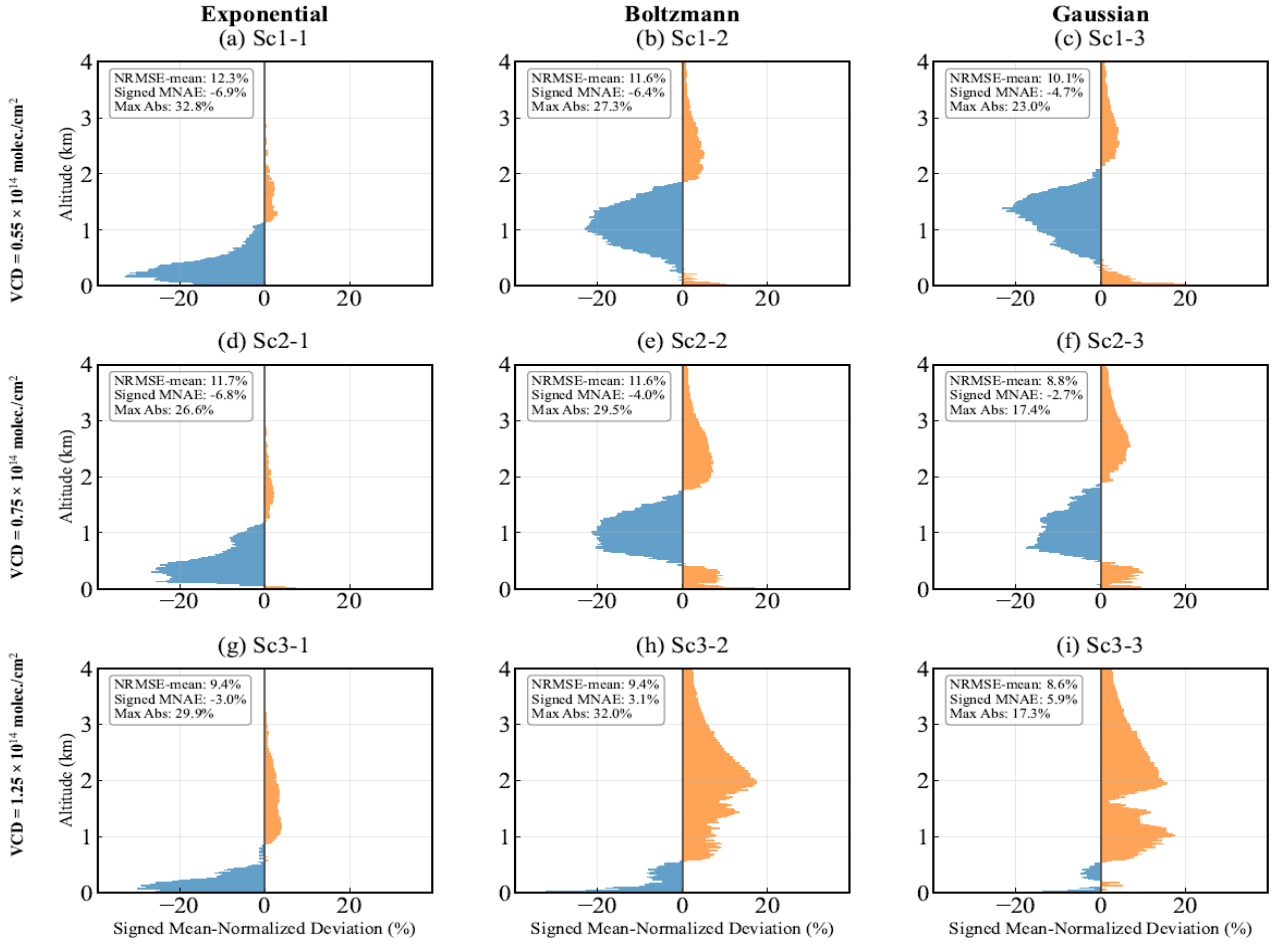


Figure 5. Mean-normalized percentage deviation vertical distributions for the nine test scenarios. Layout and scenario arrangement are identical to Figure 4. Each subplot shows the vertical distribution of percentage deviations between model predictions and true simulated profiles, annotated with three metrics: NRMSE-mean, Signed MNAE, and Max Abs.

Critically, for all unseen parameter combinations (e.g., scale height 0.35 km, boundary layer height 1.25 km), the model successfully captured core morphological features of each profile type. This demonstrates strong interpolation capability and generalization potential within the physically constrained simulation parameter space.

4.3 Validation with Independent Real MAX-DOAS Observations

4.3.1 Validation Methodology

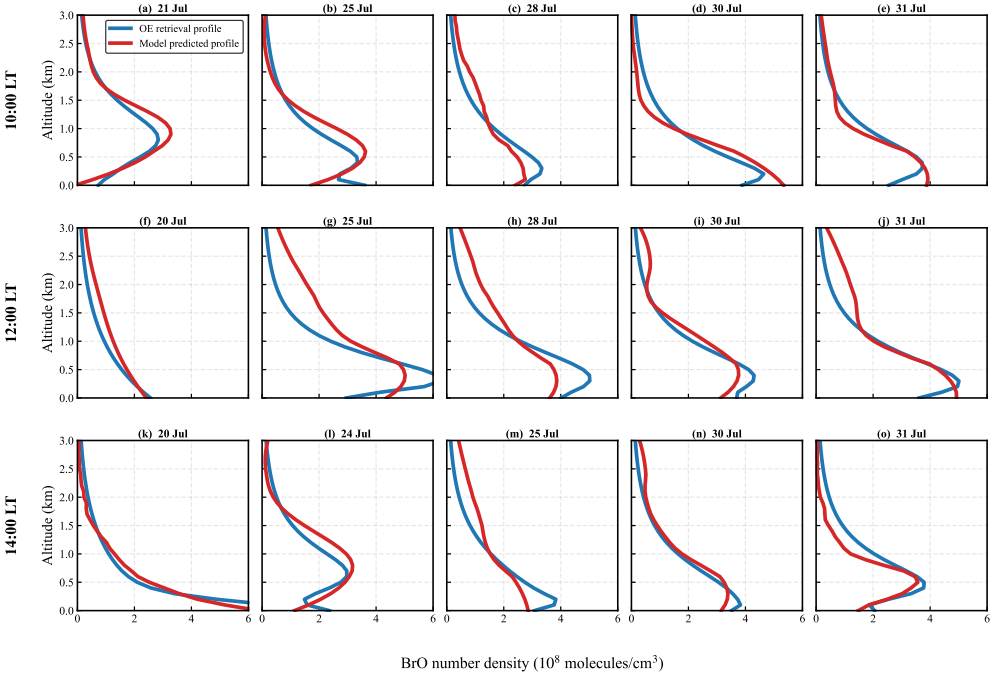
To evaluate the practical applicability of our synthetically trained model, we validated it using an independent set of real-world MAX-DOAS observations from Huaniao Island, China, in July 2018 (Wang et al., 2024a). During this period, the

https://doi.org/10.5194/egusphere-2026-5682
Preprint. Discussion started: 9 November 2026
© Author(s) 2026. CC BY 4.0 License.

station was influenced by the outer circulation of a typhoon and marine air masses, resulting in significant diurnal variations in BrO concentrations and pronounced daily changes in boundary layer structure, enabling a comprehensive assessment of the model's ability to capture the diurnal characteristics of BrO vertical distribution. To bridge the domain gap between synthetic training data and real measurements, a standardized preprocessing pipeline was applied: the measured BrO DSCD sequences were linearly interpolated to the standard elevation angles used in training, and co-located aerosol extinction profiles were mapped onto the model's fixed vertical grid (0–4 km). All input features were then standardized using the mean and standard deviation pre-computed from the synthetic training dataset, ensuring consistency with the distribution seen during training.

4.3.2 Results and Analysis

Figure 6 compares the instantaneous BrO vertical profiles retrieved by the traditional optimal-estimation (OE) method and predicted by our CNN-LSTM model at three representative times (10:00, 12:00, 14:00) across multiple days in July 2018. The model captures the main diurnal and vertical patterns. At 10:00, the BrO concentration peak typically appears at 0.5–1 km altitude. At noon (12:00), the near-surface BrO concentration increases significantly, reaching the maximum peak intensity. In the afternoon (14:00), the boundary layer is fully mixed, and the vertical gradient of the profile tends to flatten. The model-retrieved profiles are smoother than those from the OE method; at the boundary layer top and concentration peak regions where sharp gradients occur, the model predictions exhibit a slight smoothing effect, which is an inherent characteristic of deep learning models. However, the core features of the profiles, including peak height, mixed layer top position, and near-surface decay rate, are all fully consistent with the OE results.



https://doi.org/10.5194/egusphere-2026-5682
Preprint. Discussion started: 9 November 2026
© Author(s) 2026. CC BY 4.0 License.

Figure 6. Comparison of instantaneous BrO vertical profile retrievals from traditional optimal estimation (OE, blue lines) and our CNN-LSTM model (red lines) at three representative times (10:00, 12:00, 14:00) across multiple days in July 2018 at the Huaniao Island station. Panels are grouped by approximate local time: (a)–(e) 10:00 LT, (f)–(j) 12:00 LT, and (k)–(o) 14:00 LT; the date of each profile is given above the corresponding panel. The x-axis shows BrO number density (10^8 molec. cm^{-3}), and the y-axis indicates altitude (km).

To further quantify the model's performance across different photochemical stages, scatter analyses were conducted for the three representative time periods (Fig. 7). The coefficient of determination (R^2) exceeded 0.91 for all periods, with the highest value at 12:00 (0.924), followed by 10:00 (0.914) and 14:00 (0.912). However, the regression slopes revealed distinct diurnal bias patterns: the slope was closest to unity at 10:00 (1.063), indicating the best overall agreement; it decreased to 0.792 at 12:00, suggesting systematic underestimation at high concentrations due to the model's tendency toward smoother profiles under well-mixed boundary layer conditions; and it was intermediate at 14:00 (0.865). These results demonstrate the model's stable retrieval capability across varying photochemical regimes, while highlighting a moderate smoothing effect during midday when boundary layer mixing is most vigorous and BrO concentration gradients are weakest.

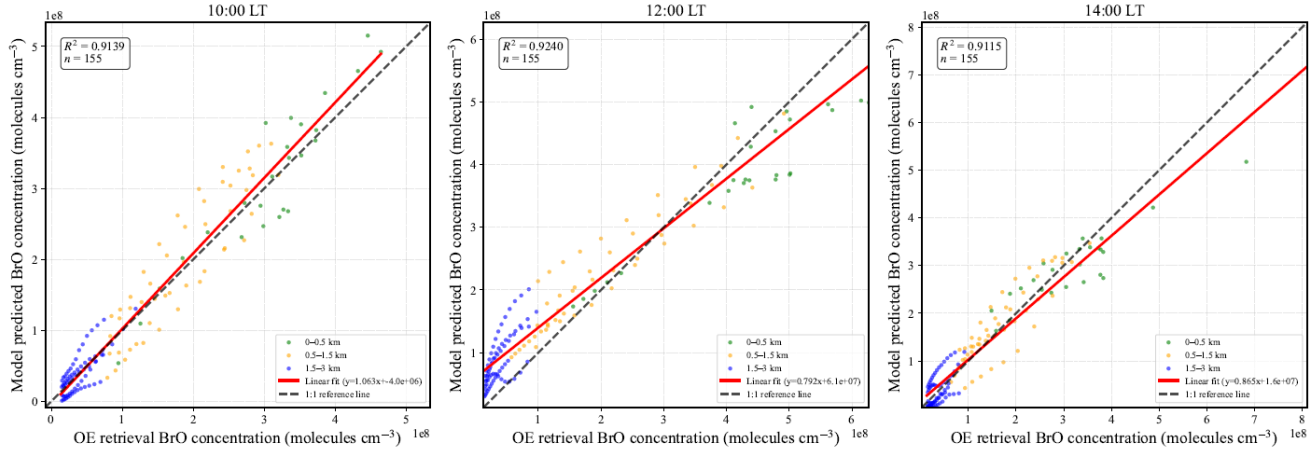


Figure 7. Scatter plots of predicted vs. OE reference BrO concentrations for three representative time periods (10:00, 12:00, 14:00) across multiple days in July 2018. The panel shows the linear fits (red lines) and 1:1 reference (black dashed line) for each time period, with regression statistics annotated.

To validate the model's overall capability in capturing the spatiotemporal distribution of BrO, July 30-31, 2018, featuring complete diurnal observation cycles, was selected as a representative case. The diurnal heatmaps (Fig. 8) demonstrate that the CNN-LSTM model reproduces the core spatiotemporal patterns of BrO, including the pronounced noon near-surface peak and the upward shift of concentration maxima during morning and evening transition periods, albeit with smoother near-surface gradients relative to the OE retrieval.

https://doi.org/10.5194/egusphere-2026-5682
Preprint. Discussion started: 9 November 2026
© Author(s) 2026. CC BY 4.0 License.

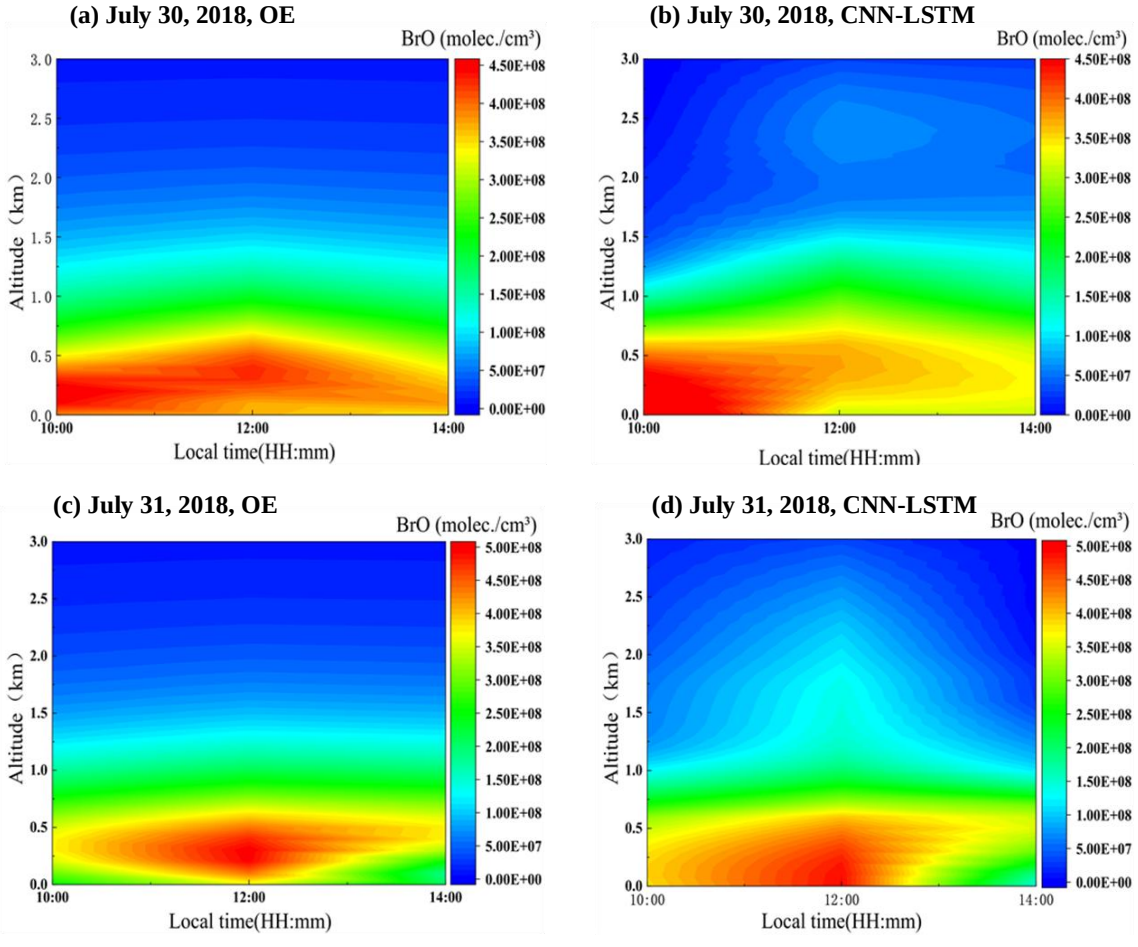


Figure 8. Daily variation heat maps of BrO profile retrieved by OE algorithm (left column) and our CNN-LSTM model (right column) from July 30 to 31, 2018. (a) and (b) are the results for July 30, 2018; (c) and (d) are the results for July 31, 2018. The color scale represents the BrO number density (molec. cm^{-3}).

The overall quantitative agreement is shown in Fig. 9. For the 186 data points (6 times × 31 altitudes), the model predictions correlate strongly with the OE reference values (slope = 0.986, R^2 = 0.9293). However, the regression intercept reveals a systematic positive bias of about 5.36×10^6 molec. cm^{-3}. Stratified by altitude, near-surface points (0–0.5 km) cluster tightly around the 1:1 line, whereas high-altitude points (1.5-3 km) show larger dispersion and a consistent positive bias, which may be attributed to the stronger dependence of the OE retrieval on a priori profile constraints, especially in the low signal-to-noise regime at higher altitudes.

https://doi.org/10.5194/egusphere-2026-5682
Preprint. Discussion started: 9 November 2026
© Author(s) 2026. CC BY 4.0 License.

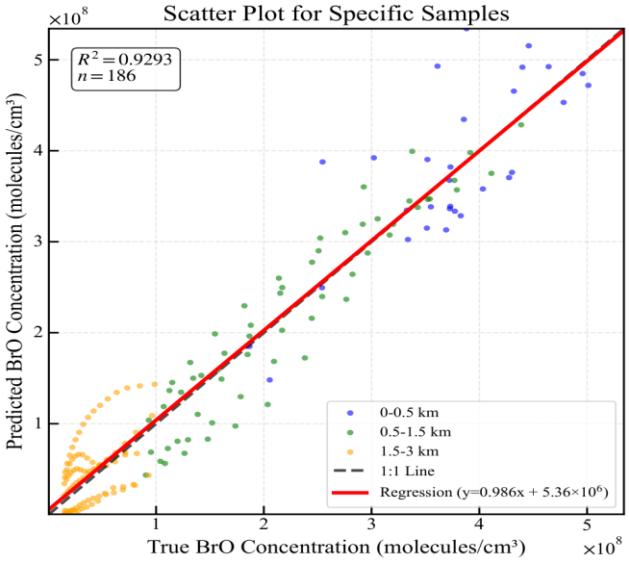


Figure 9. Predicted vs. OE reference BrO concentrations (186 points, 6 times × 31 altitudes). Colors indicate altitude: blue (0–0.5 km), green (0.5–1.5 km), orange (1.5–3 km). Black dashed line: 1:1 reference; red solid line: linear fit (y = 0.986x + 5.36 × 10^6, R^2 = 0.9293).

The bias distribution (Fig. 10) has a mean absolute bias of 3.29 × 10^6 molec. cm^{-3} and a mean relative bias of 15.84%, with a pronounced positive skew (median relative bias = 2.67%). Figure 11 further reveals the concentration and altitude dependence of retrieval errors. The absolute bias remains nearly independent of concentration, while the relative bias increases sharply at low concentrations (below 1 × 10^8 molec. cm^{-3}), explaining the observed altitude-dependent error pattern. Only 43.0% of all points fall within ±20% relative error, with most outliers occurring in the low-concentration, high-altitude regime. This concentration-dependent error characteristic is particularly pronounced in the 1.5–3 km layer, where the limited sensitivity of MAX-DOAS measurements to upper altitudes and the amplification of relative errors under low-concentration conditions jointly degrade retrieval precision.

https://doi.org/10.5194/egusphere-2026-5682
Preprint. Discussion started: 9 November 2026
© Author(s) 2026. CC BY 4.0 License.

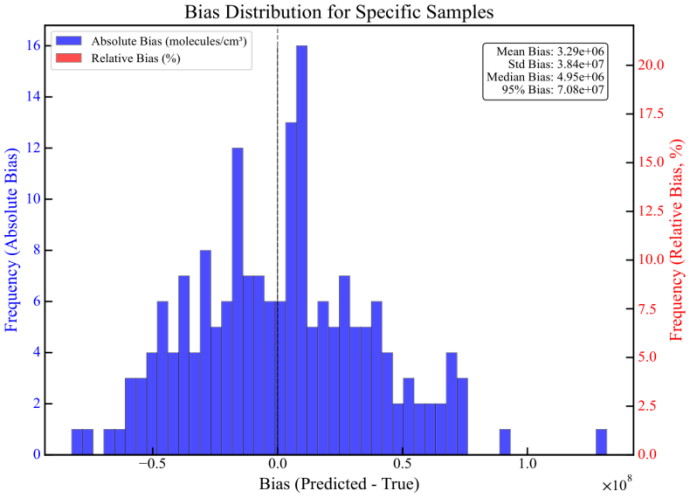


Figure 10. Distribution of retrieval biases for the CNN-LSTM model. Absolute bias (blue) and relative bias (red) are shown. Mean absolute bias = 3.29 × 10^6 molec. cm^{-3} (std: 3.84 × 10^7 molec. cm^{-3}); mean relative bias = 15.84% (std: 72.35%).

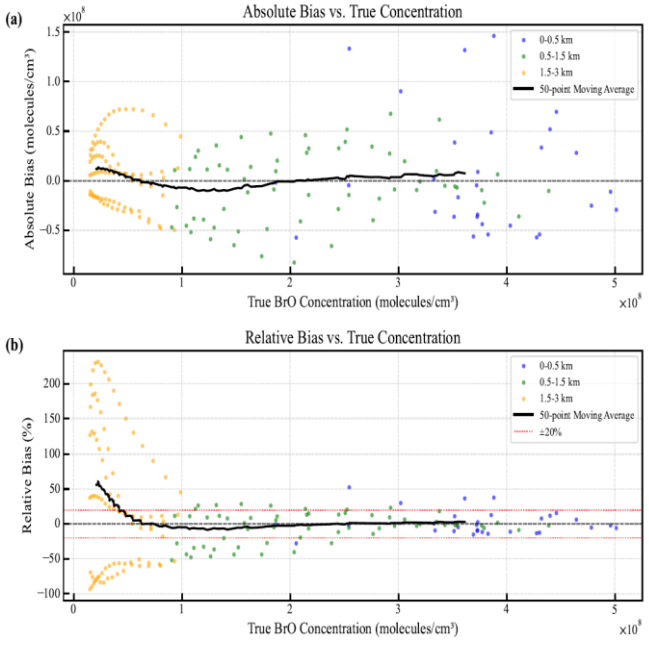


Figure 11. Absolute (a) and relative (b) bias of CNN-LSTM predictions as a function of true BrO concentration, colored by altitude: blue (0–0.5 km), green (0.5–1.5 km), orange (1.5–3 km). Black line: 50-point moving average. Dashed red lines in (b): ±20% bounds.

In summary, the model trained exclusively on synthetic data demonstrates good overall accuracy and captures the essential features of BrO variations in real MAX-DOAS observations under challenging real-world conditions. The observed biases are primarily associated with the idealized assumptions in the training simulations and the inherent difficulty of retrieving

https://doi.org/10.5194/egusphere-2026-5682
Preprint. Discussion started: 9 November 2026
© Author(s) 2026. CC BY 4.0 License.

weak absorbers at low concentrations. The method provides a fast, stable, and physically plausible alternative to conventional optimal estimation for BrO profile retrieval.

5 Discussion

5.1 Interpretation of Key Findings

A deep learning model trained exclusively on a physics-informed synthetic dataset can effectively retrieve tropospheric BrO vertical profiles, achieving performance comparable to conventional optimal estimation (OE). The model attains an R^2 of 0.84 on the synthetic validation set, demonstrating its ability to learn the mapping from multi-angle DSCDs to vertical structures. When applied to real MAX-DOAS observations at Huaniao Island in July 2018, the model produces physically plausible profiles consistent with independent OE retrievals (Wang et al., 2024a). The instantaneous profile analysis across multiple representative days at three key times (10:00, 12:00, 14:00) shows that the model accurately captures the diurnal variation characteristics and vertical distribution patterns of BrO. Furthermore, the two-day continuous diurnal cycle analysis (July 30–31) confirms the model's capability to reproduce core spatiotemporal patterns. The model addresses the ill-posed inversion step by learning from a comprehensive synthetic dataset that incorporates implicit physical constraints.

Error analysis reveals a structured bias pattern: while the median relative bias is low (2.67%), the mean relative bias (15.8%) is elevated due to positive outliers at higher altitudes. Model precision remains high (within 20%) for near-surface concentrations above 2×10^8 molec. cm^{-3}, but decreases under low-concentration conditions ($<1 \times 10^8$ molec. cm^{-3}) typical of the upper boundary layer. Despite these localized deviations, the model captures the core spatiotemporal diurnal pattern of BrO, albeit with smoother vertical gradients than OE retrievals.

5.2 Advantages and Context Compared to Traditional Retrieval

Our machine learning approach offers distinct practical advantages over conventional OE methods. First, the computational efficiency is substantially improved: a single profile retrieval requires only 0.5 s, representing a 240-fold speedup over traditional optimal estimation, while the vertical resolution of the 0–4 km output profile is enhanced to 191 layers (10 m resolution within the lowest 1 km), enabling near-real-time processing without sacrificing vertical detail. This efficiency gain is critical for applications requiring large-scale reanalysis or real-time monitoring. Second, the model learns a statistical prior from the diverse synthetic dataset, reducing subjective bias associated with a priori constraints in OE. Third, the hybrid CNN-LSTM architecture enhances robustness to noisy DSCD inputs through effective feature extraction and sequential modeling. Finally, output smoothness and physical consistency emerge inherently from the physically parameterized training profiles, avoiding ad-hoc regularization.

This work provides a scalable, data-driven framework for atmospheric profile retrieval that can be extended to other trace gases, offering a practical pathway to overcome observational data scarcity in atmospheric remote sensing.

https://doi.org/10.5194/egusphere-2026-5682
Preprint. Discussion started: 9 November 2026
© Author(s) 2026. CC BY 4.0 License.

The scope of applicability of the present development is limited by the parameter space spanned by the synthetic training dataset: cloud-free, plane-parallel atmospheric conditions, and altitudes between the surface and 4 km. Extension to other trace gases, aerosol regimes, or observation sites requires retraining with correspondingly extended radiative transfer simulations. In addition, retrieval accuracy degrades at concentrations below 1×10^8 molec. cm^{-3}, particularly above 1.5 km altitude, where the information content of MAX-DOAS observations is limited.

6 Conclusions

This study presents a novel machine learning framework, BRONet v1.0, for retrieving tropospheric BrO vertical profiles from MAX-DOAS observations, addressing the fundamental challenge of data scarcity through physics-based synthetic dataset generation. By coupling radiative transfer simulations with a hybrid CNN-LSTM architecture incorporating attention mechanisms, we demonstrate that models trained exclusively on synthetic data can achieve robust generalization to both unseen atmospheric scenarios and real-world observations. The model achieves an R^2 of 0.84 on synthetic validation data. In independent validation against real MAX-DOAS observations at Huaniao Island, China, in July 2018, the model demonstrates strong retrieval performance: instantaneous profile analysis across multiple representative days at three key times (10:00, 12:00, 14:00) confirms accurate capture of diurnal variation characteristics and vertical distribution patterns; statistical validation from two complete diurnal cycles (July 30–31) yields an overall R^2 of 0.9293 with a mean relative deviation of 15.8% compared to traditional optimal estimation retrievals. These results establish the viability of synthetic training data as a viable pathway for advancing data-driven atmospheric remote sensing, particularly for trace gases with limited observational records.

Code and data availability

The tropospheric bromine monoxide radical vertical profiles and their differential slant column densities (DSCD) dataset based on forward simulations with an atmospheric radiative transfer model is available from the Science Data Bank at https://doi.org/10.57760/sciencedb.27958 (Huang, 2025). The dataset includes all 51.5 million samples used for training and validation, stored in Apache Parquet format. The training code for BrO vertical profile retrieval using a CNN-LSTM model with an attention mechanism is available from the Science Data Bank at https://doi.org/10.57760/sciencedb.32920 under a CC BY 4.0 licence (Huang, 2026). The MAX-DOAS observational data from Huaniao Island, China have been deposited in the Science Data Bank (ScienceDB) and are openly available at https://www.scidb.cn/s/uAVFNr. The trained CNN-LSTM model for BrO vertical profile retrieval is available at https://www.scidb.cn/s/N7RV3e. The code is implemented in Python using TensorFlow 2.15. Both the dataset and the code are published in persistent public archives with unique identifiers.

https://doi.org/10.5194/egusphere-2026-5682
Preprint. Discussion started: 9 November 2026
© Author(s) 2026. CC BY 4.0 License.

Author contributions

ZH developed the model, performed simulations and analysis, and drafted the manuscript. XT designed the study, supervised the research, and secured funding. PX and SW provided experimental guidance and data support. YH and ZL assisted with data processing. WL provided scientific oversight. All authors reviewed and approved the final manuscript.

Competing interests

The authors declare that they have no conflict of interest.

Financial support

This research has been supported by the National Key Research and Development Program of China (grant nos. 2022YFC3700303).

References

Bartlett, P. L. and Baxter, J.: Estimation and approximation bounds for gradient-based reinforcement learning, J. Comput. Syst. Sci., 64, 133–150, https://doi.org/10.1006/jcss.2001.1793, 2002.

Coburn, S., Dix, B., Sinreich, R., and Volkamer, R.: The CU ground MAX-DOAS instrument: characterization of RMS noise limitations and first measurements near Pensacola, FL, of BrO, IO, and CHOCHO, Atmos. Meas. Tech., 4, 2421–2439, https://doi.org/10.5194/amt-4-2421-2011, 2011.

Dong, Y., Spinei, E., and Karpatne, A.: A feasibility study to use machine learning as an inversion algorithm for aerosol profile and property retrieval from multi-axis differential absorption spectroscopy measurements, Atmos. Meas. Tech., 13, 5537–5550, https://doi.org/10.5194/amt-13-5537-2020, 2020.

Dubovik, O., Holben, B., Eck, T. F., Smirnov, A., Kaufman, Y. J., King, M. D., Tanré, D., and Slutsker, I.: Variability of absorption and optical properties of key aerosol types observed in worldwide locations, J. Atmos. Sci., 59, 590–608, https://doi.org/10.1175/1520-0469(2002)059<0590:VOAAOP>2.0.CO;2, 2002.

Efremenko, D. S., Loyola, D. G., Hedelt, P., and Spurr, R. J. D.: Volcanic SO2 plume height retrieval from UV sensors using a full-physics inverse learning machine algorithm, Int. J. Remote Sens., 38, 1–27, https://doi.org/10.1080/01431161.2017.1348644, 2017.

Frieß, U., Beirle, S., Alvarado Bonilla, L., Bösch, T., Friedrich, M. M., Hendrick, F., Piters, A., Richter, A., van Roozendael, M., Rozanov, V. V., Spinei, E., Tirpitz, J.-L., Vlemmix, T., Wagner, T., and Wang, Y.: Intercomparison of MAX-DOAS vertical profile retrieval algorithms: studies using synthetic data, Atmos. Meas. Tech., 12, 2155–2181, https://doi.org/10.5194/amt-12-2155-2019, 2019.

https://doi.org/10.5194/egusphere-2026-5682
Preprint. Discussion started: 9 November 2026
© Author(s) 2026. CC BY 4.0 License.

Gers, F. A., Schmidhuber, J., and Cummins, F.: Learning to forget: continual prediction with LSTM, Neural Comput., 12, 2451–2471, https://doi.org/10.1162/089976600300015015, 2000.

Gliß, J., Bobrowski, N., Vogel, L., Pöhler, D., and Platt, U.: OClO and BrO observations in the volcanic plume of Mt. Etna – implications on the chemistry of chlorine and bromine species in volcanic plumes, Atmos. Chem. Phys., 15, 5659–5681, https://doi.org/10.5194/acp-15-5659-2015, 2015.

Hedelt, P., Efremenko, D. S., Loyola, D. G., Spurr, R., and Clarisse, L.: Sulfur dioxide layer height retrieval from Sentinel-5 Precursor/TROPOMI using FP_ILM, Atmos. Meas. Tech., 12, 5503–5517, https://doi.org/10.5194/amt-12-5503-2019, 2019.

Huang, Z.: Tropospheric bromine monoxide radical vertical profiles and their differential slant column densities (DSCD) dataset based on forward simulations with an atmospheric radiative transfer model, Science Data Bank [data set], https://doi.org/10.57760/sciencedb.27958, 2025.

Huang, Z.: Training code for BrO vertical profile retrieval using a CNN-LSTM model with attention mechanism, Science Data Bank [code], https://doi.org/10.57760/sciencedb.32920, 2026.

Hönninger, G., von Friedeburg, C., and Platt, U.: Multi axis differential optical absorption spectroscopy (MAX-DOAS), Atmos. Chem. Phys., 4, 231–254, https://doi.org/10.5194/acp-4-231-2004, 2004.

Pan, Y., Tian, X., Xie, P., Li, A., Xu, J., Ren, B., Huang, X., Tian, W., and Wang, Z.: Prediction of tropospheric NO2 profile using CNN-SVR for MAX-DOAS spectrum, Acta Opt. Sin., 42, 2401001, https://doi.org/10.3788/aos202242.2401001, 2022.

Peterson, P. K., Simpson, W. R., Pratt, K. A., Shepson, P. B., Frieß, U., Zielcke, J., Platt, U., Walsh, S. J., and Nghiem, S. V.: Dependence of the vertical distribution of bromine monoxide in the lower troposphere on meteorological factors such as wind speed and stability, Atmos. Chem. Phys., 15, 2119–2137, https://doi.org/10.5194/acp-15-2119-2015, 2015.

Rozanov, A., Rozanov, V., Buchwitz, M., Kokhanovsky, A., and Burrows, J. P.: SCIATRAN 2.0 – A new radiative transfer model for geophysical applications in the 175–2400 nm spectral region, Adv. Space Res., 36, 1015–1019, https://doi.org/10.1016/j.asr.2005.03.012, 2005.

Schilling, H., Bulatov, D., Niessner, R., Middelmann, W., and Soergel, U.: Detection of vehicles in multisensor data via multibranch convolutional neural networks, IEEE J. Sel. Top. Appl. Earth Obs. Remote Sens., 11, 4299–4316, https://doi.org/10.1109/JSTARS.2018.2825099, 2018.

Sellitto, P., Bojkov, B. R., Liu, X., Chance, K., and Del Frate, F.: Tropospheric ozone column retrieval at northern mid-latitudes from the Ozone Monitoring Instrument by means of a neural network algorithm, Atmos. Meas. Tech., 4, 2375–2388, https://doi.org/10.5194/amt-4-2375-2011, 2011.

Simpson, W. R., Peterson, P. K., Frieß, U., Sihler, H., Lampel, J., Platt, U., Moore, C., Pratt, K., Shepson, P., Halfacre, J., and Nghiem, S. V.: Horizontal and vertical structure of reactive bromine events probed by bromine monoxide MAX-DOAS, Atmos. Chem. Phys., 17, 9291–9309, https://doi.org/10.5194/acp-17-9291-2017, 2017.

Tian, L., Feng, L., Yang, L., and Guo, Y.: Stock price prediction based on LSTM and LightGBM hybrid model, J. Supercomput., 78, 11768-11793, https://doi.org/10.1007/s11227-022-04326-5, 2022.

https://doi.org/10.5194/egusphere-2026-5682
Preprint. Discussion started: 9 November 2026
© Author(s) 2026. CC BY 4.0 License.

Tian, X., Wang, Y., Beirle, S., Xie, P., Wagner, T., Xu, J., Li, A., Dörner, S., Ren, B., and Li, X.: Technical note: Evaluation of profile retrievals of aerosols and trace gases for MAX-DOAS measurements under different aerosol scenarios based on radiative transfer simulations, Atmos. Chem. Phys., 21, 12867–12894, https://doi.org/10.5194/acp-21-12867-2021, 2021.

Wagner, T., Ibrahim, O., Sinreich, R., Frieß, U., von Glasow, R., and Platt, U.: Enhanced tropospheric BrO over Antarctic sea ice in mid-winter observed by MAX-DOAS on board the research vessel Polarstern, Atmos. Chem. Phys., 7, 3129-3142, https://doi.org/10.5194/acp-7-3129-2007, 2007.

Wang, S., Li, Q., Zhang, R., Mahajan, A. S., Inamdar, S., Benavent, N., Zhang, S., Xue, R., Zhu, J., Jin, C., Zhang, Y., Fu, X., Badia, A., Fernandez, R. P., Cuevas, C. A., Wang, T., Zhou, B., and Saiz-Lopez, A.: Typhoon- and pollution-driven enhancement of reactive bromine in the mid-latitude marine boundary layer, Natl. Sci. Rev., 11, 93--101, https://doi.org/10.1093/nsr/nwae074, 2024.

Wang, Z., Tian, X., Xie, P., Xu, J., Zheng, J., Pan, Y., Zhang, T., and Fan, G.: A convolutional neural networks method for tropospheric ozone vertical distribution retrieval from multi-axis differential optical absorption spectroscopy measurements, Sci. Total Environ., 951, 175049, https://doi.org/10.1016/j.scitotenv.2024.175049, 2024.

Zhang, S., Wang, S., Zhu, J., Xue, R., Jiang, Z., Gu, C., Yan, Y., and Zhou, B.: Stacking machine learning models empowered high time-height-resolved ozone profiling from the ground to the stratopause based on MAX-DOAS observation, Environ. Sci. Technol., 58, 7433-7444, https://doi.org/10.1021/acs.est.3c09099, 2024.